

Supporting Information

Phosphonate-assisted Tetranuclear Lanthanide Assemblies: Observation Of Toroidic Ground State in the Tb^{III} Analogue

*Sourav Biswas,^a Pawan Kumar,^b Abinash Swain,^c Tulika Gupta,^c Pankaj Kalita,^e Subrata Kundu,^b Gopalan Rajaraman^{*c} and Vadapalli Chandrasekhar^{*b,d}*

^aDepartment of Geo-Chemistry, Keshav Deva Malaviya Institute of Petroleum Exploration, Dehradun-248915, India.

^bDepartment of Chemistry, Indian Institute of Technology Kanpur, Kanpur-208016, India

^cDepartment of Chemistry, Indian Institute of Technology Bombay, Powai, Mumbai 400076.

^dTata Institute of Fundamental Research, Gopanpally, Hyderabad - 500 107, India,

^eSchool of Chemical Sciences, National Institute of Science Education and Research Bhubaneswar, HBNI, Jatni, Khurda – 752050, India.

AUTHOR EMAIL ADDRESS: vc@iitk.ac.in; ; vc@tifrh.res.in; rajaraman@chem.iitb.ac.in

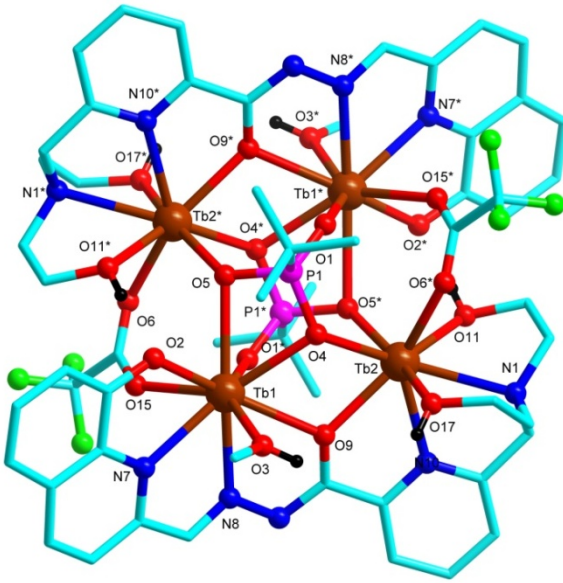


Figure S1. Molecular Structure of compound 2 (selected hydrogen atoms, chlorides and non-coordinated solvent molecules were omitted for clarity).

Table S1. Selected Bond Distances (\AA) and Bond angles ($^{\circ}$) for compound 2

Bond distances around Tb1	Bond distances around Tb2	Bond angles around Tb			
Tb(1)-O(1)	2.268(3)	Tb(2)-O(5)	2.299(3)	Tb(2)-O(4)-Tb(1)	112.66(11)
Tb(1)-O(2)	2.357(3)	Tb(2)-O(6)	2.355(3)	Tb(2)-O(5)-Tb(1)*	118.06(11)
Tb(1)-O(3)	2.390(3)	Tb(2)-O(17)	2.355(3)	Tb(2)-O(9)-Tb(1)	111.99(11)
Tb(1)-O(15)*	2.414(3)	Tb(2)-O(9)	2.374(3)		
Tb(1)-O(4)	2.494(3)	Tb(2)-O(4)	2.394(3)		
Tb(1)-O(9)	2.533(3)	Tb(2)-O(11)	2.403(3)		
Tb(1)-N(8)	2.554(4)	Tb(2)-N(10)	2.572(4)		
Tb(1)-N(7)	2.559(4)	Tb(2)-N(1)	2.683(4)		
Tb(1)-O(5)*	2.647(3)				

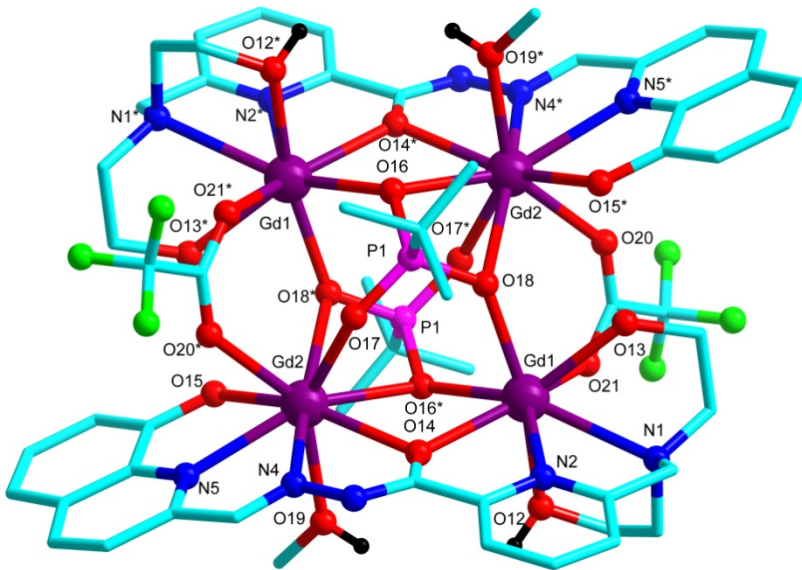


Figure S2. Molecular Structure of compound 3 (selected hydrogen atoms, chlorides and non-coordinated solvent molecules were omitted for clarity).

Table S2. Selected Bond Distances (\AA) and Bond angles ($^{\circ}$) for compound 3

Bond distances around Gd1	Bond distances around Gd2	Bond angles around Gd
Gd(1)-O(18)	2.331(3)	Gd(1)*-O(16)-Gd(2)* 112.53(12)
Gd(1)-O(21)*	2.370(3)	Gd(1)-O(14)-Gd(2) 111.68(12)
Gd(1)-O(12)	2.373(4)	Gd(1)-O(18)-Gd(2)* 117.84(13)
Gd(1)-O(14)	2.393(3)	
Gd(1)-O(16)*	2.401(3)	
Gd(1)-O(13)	2.422(3)	
Gd(1)-N(2)	2.585(4)	
Gd(1)-N(1)	2.689(4)	
	Gd(2)-O(17) 2.288(3)	
	Gd(2)-O(15) 2.375(3)	
	Gd(2)-O(19) 2.408(3)	
	Gd(2)-O(20) 2.421(4)	
	Gd(2)-O(16)* 2.506(3)	
	Gd(2)-O(14) 2.539(3)	
	Gd(2)-N(4) 2.565(4)	
	Gd(2)-N(5) 2.583(4)	
	Gd(2)-O(18)* 2.627(3)	

The crystal packing analysis of **1** reveals the presence of intramolecular as well as intermolecular hydrogen bonding interactions. Two sets of intramolecular hydrogen bonding are encountered in **1**: in one set, two strong hydrogen bonding are formed between the $-\text{CH}_2\text{CH}_2\text{OH}$ of a $[\text{LH}_2]^{2-}$ and the O of the 8-hydroxyquinoline of the adjacent $[\text{LH}_2]^{2-}$ with D-H.....A, 1.814 \AA while in other set the two chloride counter anions are flanked by two pairs of hydrogen bonding

interactions (two $-\text{CH}_2\text{CH}_2\text{OH} \dots \text{Cl}$ (2.086 \AA) and two $\text{CH}_3\text{OH} \dots \text{Cl}$ (2.211 \AA) interactions) (Figure S3). We suggest that these interactions prevent the de-protonation of the $-\text{CH}_2\text{CH}_2\text{OH}$ arms of the ligand.

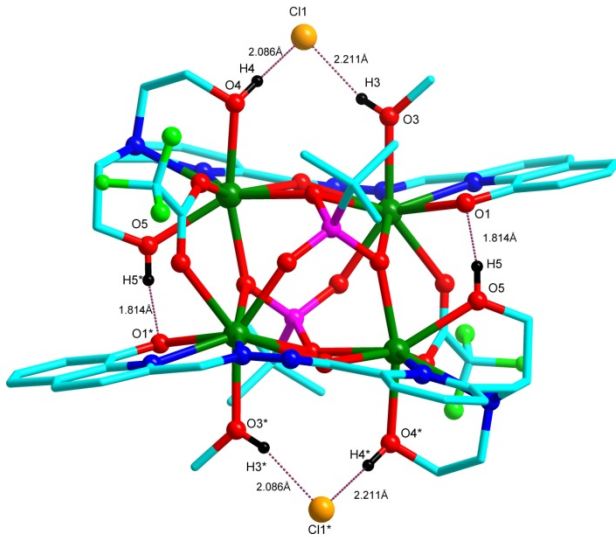


Figure S3: Two set of intramolecular hydrogen bonding of complex **1** (selected hydrogen atoms, and the solvent molecules have been omitted for clarity).

An analysis of the crystal packing **1** reveals that it is possible to hierarchically construct its supramolecular structure. First a 1D chain is generated as a result of a pair of intermolecular hydrogen bonding interactions between the hydrazine N and para Ar–H mediated by a solvent methanol molecule (Figure S4). Bond parameters involved in this hydrogen bonding are given in

Table S3.

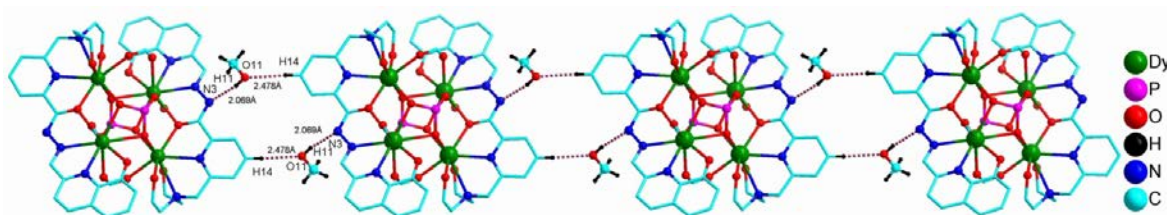


Figure S4. 1D supramolecular structure of complex **1** (selected carbon, hydrogen, chloride, fluorine and solvent molecules are omitted for clarity).

Also, a 2D network formation was observed in **1** due to presence of two set of intermolecular hydrogen bonding: in one set each complex is connected to other via a pair of hydrogen bonding between F and C–H of $-\text{CH}_2\text{CH}_2\text{OH}$ giving rise to a 1D chain while in other set two such 1D chain are connected to each other through three intermolecular hydrogen bonding which involve a Cl and a Ar–H of the 8-hydroxy quinoline, OH of a $-\text{CH}_2\text{CH}_2\text{OH}$ and OH of the coordinated MeOH (Figure S5).

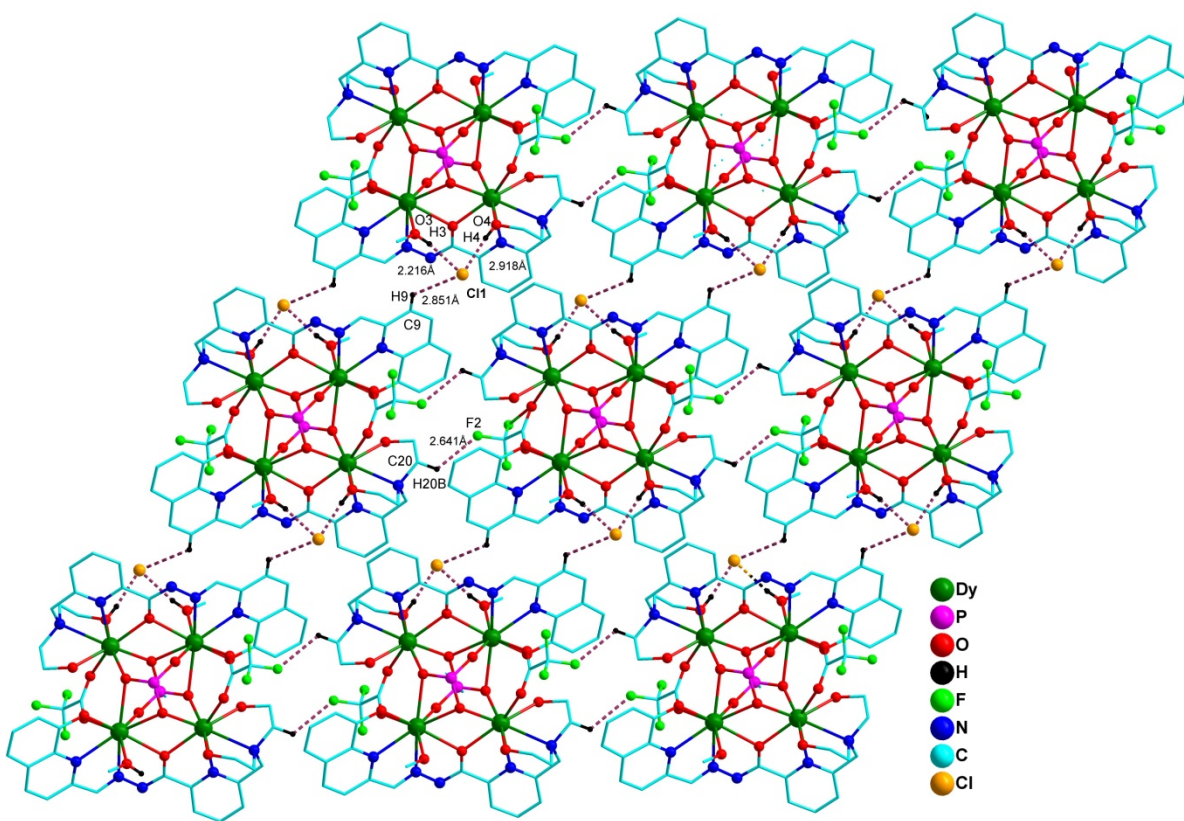


Figure S5. 2D supramolecular structure of complex **1** (selected carbon, hydrogen, chloride and solvent molecules are omitted for clarity).

Table S3: Hydrogen bond parameter for complex **1**.

D–H....A	d(D–H)	d(H....A)	d(D....A)	<(DHA)	Symmetry
	(Å)	(Å)	(Å)	(°)	
C14–H14...O11	0.930	2.478	3.381	163.65	1-x,1-y, 2-z
O11–H11....N3	0.821	2.069	2.878	168.03	1+x, y, 1+z
O3–H3...Cl1	0.840	2.216	3.047	166.92	
O4–H4...Cl1	0.860	2.918	2.918	163.13	
C9–H9... Cl1	0.950	2.851	3.509	127.41	
C20–H20B....F2	0.990	2.641	3.245	119.55	

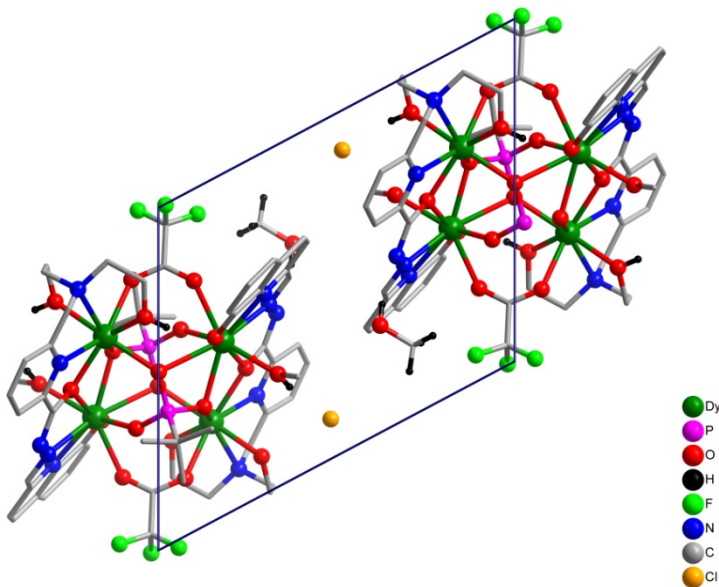


Figure S6. Crystal packing along the x axis.

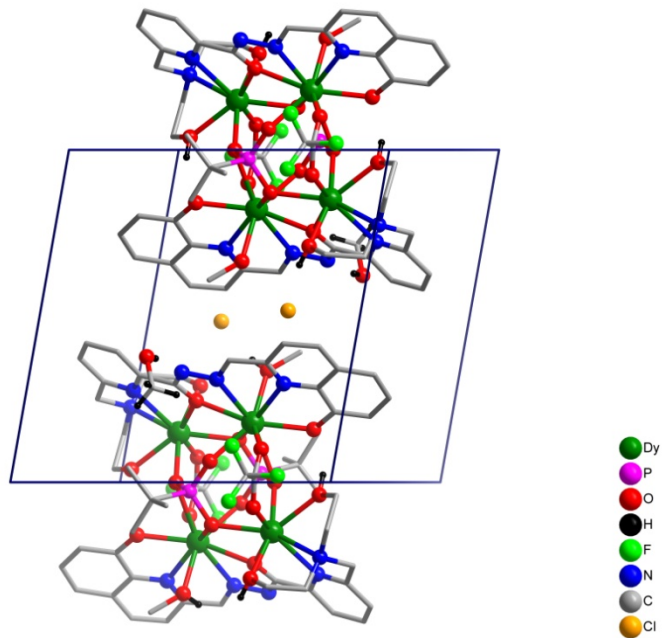


Figure S7. Crystal packing along the Y axis.

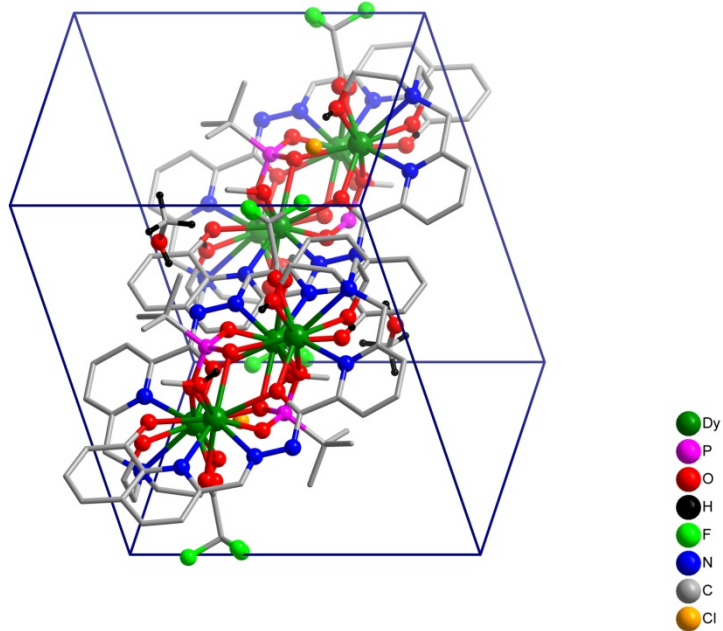


Figure S8. Crystal packing along the Y axis

Table S4. CASSCF+RASSI-SO+SINGLE_ANISO computed energies of the eight low-lying KDs of the each Dy centres along with the main values of the g-tensors of ground state KD in complex **1**.

Complex 1	Energies of KD _s @Dy1 (cm ⁻¹)	Energies of KD _s @Dy2 (cm ⁻¹)	Energies of KD _s @Dy3 (cm ⁻¹)	Energies of KD _s @Dy4 (cm ⁻¹)
KD1	0.000	0.000	0.000	0.000
	0.000	0.000	0.000	0.000
KD2	76.719	142.098	76.716	142.098
	76.719	142.098 233.154	76.716	142.098
KD3	132.235	233.154 328.543	133.235	233.154
	132.235	328.543	133.235	233.154
KD4	168.587	411.255 411.255	165.586	328.543
	168.587	450.186	165.586	328.543
KD5	209.368	450.186 536.466	209.368	411.255
	209.368	536.466	209.368	411.255
KD6	304.232	640.867 640.867	304.232	450.186
	304.232		304.232	450.186
KD7	371.082		371.081	536.466
	371.082		371.081	536.466
KD8	401.422		401.422	640.867
	401.422		401.422	640.867
	Main values of the ground state g-tensors			
	g _x = 0.118 g _y = 0.306	g _x = 0.013 g _y = 0.025	g _x = 0.118 g _y = 0.306	g _x = 0.013 g _y = 0.025

	$g_z = 19.118$	$g_z = 19.698$	$g_z = 19.063$	$g_z = 19.728$
--	----------------	----------------	----------------	----------------

Table S5. SINGLE_ANISO computed crystal field parameters for the Dy ions in complex **1**. The major components in the Table are in bold. B_k^q is the crystal field parameter and O_k^q is the extended Stevens operator. The quantization axis is chosen to be the main magnetic axis of the ground Kramer's Doublet.

k	q	B_k^q	B_k^q	B_k^q	B_k^q
		Dy1	Dy2	Dy3	Dy4
2	-2	-1.09	1.05	-1.09	1.05
2	-1	0.43	-0.12	0.45	-0.13
2	0	-1.22	-3.02	-1.22	-3.02
2	1	1.13	0.85	1.11	0.83
2	2	0.58	1.14	0.58	1.14
4	-4	-0.61×10^{-2}	-0.23×10^{-2}	-0.59×10^{-2}	-0.25×10^{-2}
4	-3	0.46×10^{-1}	-0.40×10^{-1}	0.45×10^{-1}	-0.39×10^{-1}
4	-2	0.17×10^{-1}	0.91×10^{-2}	0.17×10^{-1}	0.90×10^{-2}
4	-1	-0.11×10^{-2}	0.69×10^{-2}	-0.11×10^{-2}	0.66×10^{-2}
4	0	-0.18×10^{-2}	0.78×10^{-4}	-0.18×10^{-2}	0.74×10^{-4}
4	1	0.78×10^{-2}	0.10×10^{-1}	0.75×10^{-2}	0.10×10^{-1}
4	2	0.91×10^{-2}	0.18×10^{-2}	0.90×10^{-2}	0.17×10^{-2}
4	3	0.21×10^{-1}	0.50×10^{-1}	0.20×10^{-1}	0.51×10^{-1}
4	4	0.39×10^{-1}	-0.17×10^{-1}	0.40×10^{-1}	-0.17×10^{-1}
6	-6	-0.11×10^{-3}	-0.95×10^{-4}	-0.11×10^{-3}	-0.96×10^{-4}
6	-5	-0.41×10^{-3}	-0.16×10^{-3}	-0.41×10^{-3}	-0.16×10^{-3}
6	-4	-0.97×10^{-4}	0.18×10^{-3}	-0.99×10^{-4}	0.18×10^{-3}

6	-3	0.68×10^{-4}	0.43×10^{-3}	0.68×10^{-4}	0.42×10^{-3}
6	-2	0.12×10^{-3}	-0.13×10^{-3}	0.13×10^{-3}	-0.13×10^{-3}
6	-1	-0.45×10^{-5}	-0.84×10^{-4}	0.12×10^{-6}	-0.87×10^{-4}
6	0	-0.32×10^{-4}	-0.16×10^{-4}	-0.32×10^{-4}	-0.16×10^{-4}
6	1	-0.20×10^{-3}	-0.22×10^{-3}	-0.20×10^{-3}	-0.22×10^{-3}
6	2	-0.12×10^{-3}	0.12×10^{-3}	-0.12×10^{-3}	0.12×10^{-3}
6	3	-0.11×10^{-3}	0.21×10^{-3}	-0.11×10^{-3}	0.21×10^{-3}
6	4	0.49×10^{-4}	-0.20×10^{-3}	0.49×10^{-4}	-0.20×10^{-3}
6	5	-0.26×10^{-3}	-0.16×10^{-4}	-0.24×10^{-3}	-0.16×10^{-4}
6	6	-0.38×10^{-4}	0.11×10^{-3}	-0.39×10^{-4}	0.11×10^{-3}

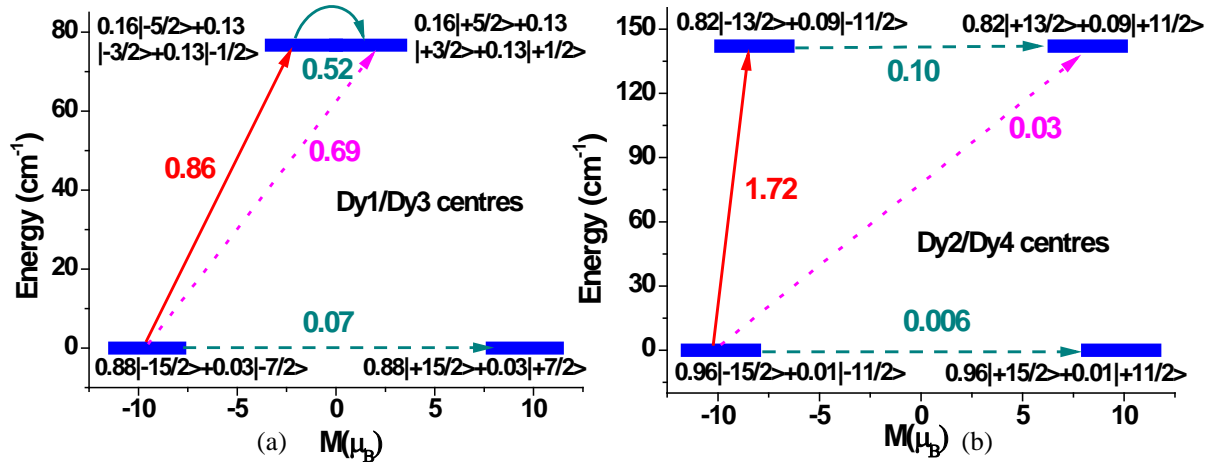


Figure S9. *Ab initio* calculated magnetization relaxation mechanism for a) Dy1/Dy3 and b) Dy2/Dy4 centres respectively in **1**.

Table S6. CASSCF+RASSI-SO+SINGLE_ANISO computed energies of the thirteen energy levels of the each Tb centres along with the main values of the g-tensors of pseudo-doublets in complex **2**:

Levels	Energies of pseudo-doublets	Energies of pseudo-doublets	Energies of pseudo-doublets	Energies of pseudo-doublets
--------	-----------------------------	-----------------------------	-----------------------------	-----------------------------

	@Tb1 (cm ⁻¹)	@Tb2 (cm ⁻¹)	@Tb3 (cm ⁻¹)	@Tb4 (cm ⁻¹)
1	0.000	0.000	0.000	0.000
2	0.036	0.991	0.036	0.989
3	157.294	47.375	157.376	47.394
4	157.889	55.424	157.970	55.443
5	320.074	105.404	320.204	105.408
6	325.796	113.538	325.918	113.540
7	443.399	153.201	443.581	153.208
8	474.851	190.612	474.988	190.605
9	524.547	201.909	524.724	201.908
10	579.489	297.062	579.705	297.067
11	588.709	300.961	588.929	300.966
12	735.560	382.362	735.912	382.353
13	736.223	384.161	736.574	384.152
Main values of the ground state g-tensors				
	g _x = 0.000	g _x = 0.000	g _x = 0.0	g _x = 0.0
	g _y = 0.000	g _y = 0.000	g _y = 0.0	g _y = 0.0
	g _z = 17.891	g _z = 17.186	g _z = 17.871	g _z = 17.179

Table S7. SINGLE_ANISO computed crystal field parameters for the Dy ions in complex **1**. The major components in the Table are in bold. B_k^q is the crystal field parameter and O_k^q is the extended Stevens operator. The quantization axis is chosen to be the main magnetic axis of the ground Kramers Doublet.

k	q	B_k^q	B_k^q	B_k^q	B_k^q
		Tb1	Tb2	Tb3	Tb4

2	-2	1.32	-0.62	-1.33	-1.27
2	-1	-1.50	-1.72	2.23	-3.79
2	0	-6.09	-2.00	-6.09	-2.00
2	1	-2.20	-3.38	-1.49	0.15
2	2	-2.75	-2.22	-2.76	1.94
4	-4	-0.13×10^{-1}	-0.16×10^{-1}	-0.12×10^{-1}	-0.26×10^{-1}
4	-3	-0.93×10^{-1}	0.25	0.57×10^{-1}	-0.20
4	-2	-0.58 x 10⁻²	-0.22×10^{-1}	0.61×10^{-2}	0.20×10^{-1}
4	-1	0.12×10^{-1}	0.93×10^{-2}	-0.29×10^{-1}	0.34×10^{-1}
4	0	0.18×10^{-2}	-0.38×10^{-2}	0.18×10^{-2}	-0.38×10^{-2}
4	1	0.29×10^{-1}	0.34×10^{-1}	0.12 x 10⁻¹	0.54 x 10⁻²
4	2	-0.75×10^{-3}	0.73×10^{-2}	0.40×10^{-3}	0.12×10^{-1}
4	3	0.57 x 10⁻¹	-0.12	0.93×10^{-1}	0.19
4	4	0.33×10^{-1}	0.28×10^{-1}	0.33×10^{-1}	-0.19×10^{-1}
6	-6	0.54×10^{-4}	0.83×10^{-4}	-0.54×10^{-4}	-0.28×10^{-4}
6	-5	-0.18×10^{-3}	-0.90×10^{-3}	-0.26×10^{-5}	-0.61×10^{-3}
6	-4	-0.14×10^{-4}	-0.61×10^{-4}	-0.14×10^{-3}	-0.16×10^{-4}
6	-3	0.23×10^{-3}	-0.23×10^{-3}	0.19×10^{-3}	0.96×10^{-4}
6	-2	1.00×10^{-4}	0.98×10^{-5}	-0.11×10^{-3}	0.12×10^{-3}
6	-1	0.89×10^{-4}	0.46×10^{-4}	0.18×10^{-3}	-0.56×10^{-4}
6	0	0.35×10^{-4}	-0.12×10^{-4}	0.35×10^{-4}	-0.12×10^{-4}
6	1	-0.18×10^{-3}	-0.83×10^{-4}	0.85×10^{-4}	-0.73×10^{-4}
6	2	-0.12×10^{-3}	0.16×10^{-3}	0.14×10^{-3}	-0.11×10^{-3}
6	3	0.20×10^{-3}	0.33×10^{-3}	-0.20×10^{-3}	-0.43×10^{-3}

6	4	-0.13×10^{-4}	0.31×10^{-4}	-0.15×10^{-4}	-0.74×10^{-4}
6	5	-0.12×10^{-4}	-0.28×10^{-3}	-0.18×10^{-3}	-0.71×10^{-3}
6	6	0.12×10^{-4}	-0.17×10^{-3}	-0.11×10^{-4}	-0.19×10^{-3}

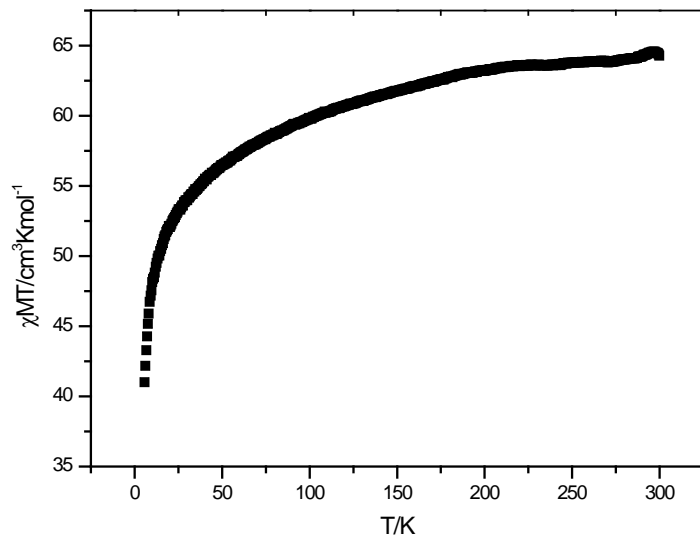


Figure S10. The Temperature T vs γT for complexes **1** at 1.0 T.

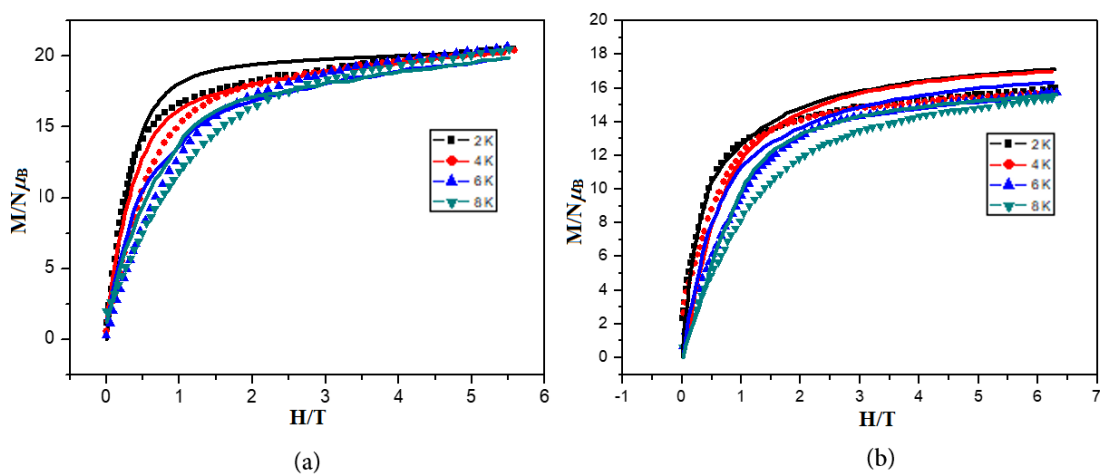


Figure S11. Field dependence of molar magnetization plot in complexes a) **1** and b) **2** in 0.1 T

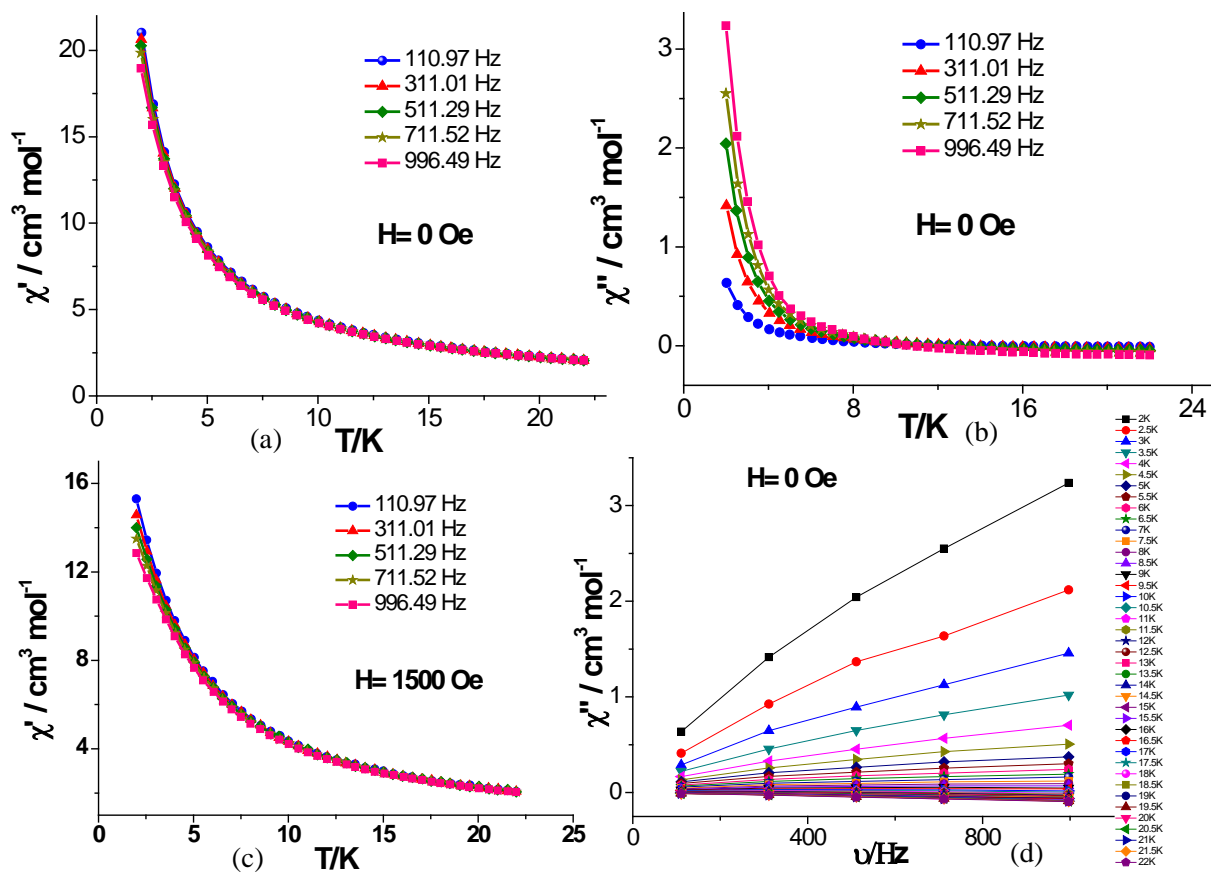


Figure S12. Temperature dependence of the a) in phase and b) out-of-phase ac susceptibility at 0 T dc applied magnetic field for complex **1**. Temperature dependence of the c) in phase ac susceptibility at 0.15 T dc applied magnetic field for complex **1**. Frequency dependence of the out-of-phase ac susceptibility at d) 0.15 T dc applied magnetic field for complex **1**.

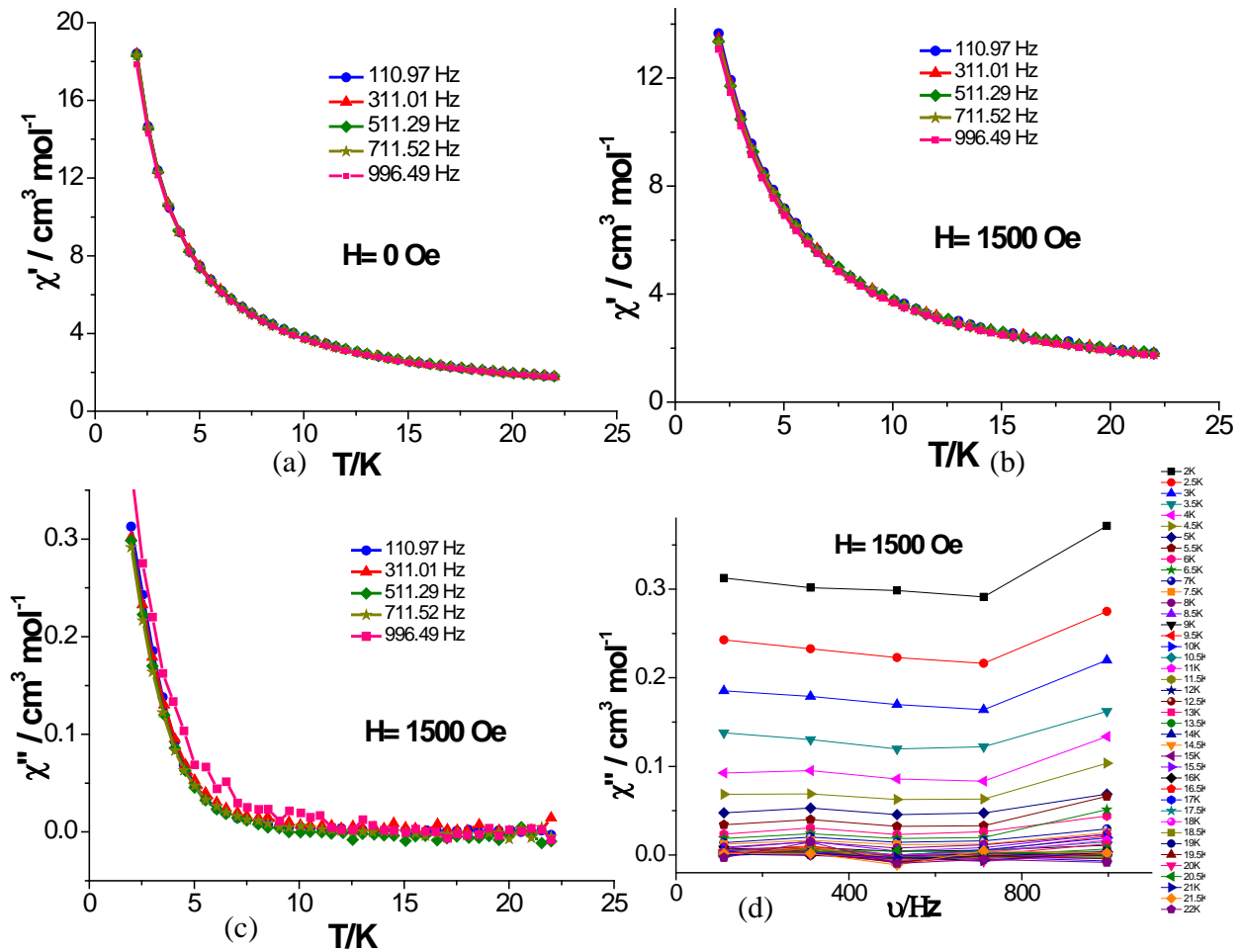


Figure S13. Temperature dependence of the in ac susceptibility at a) 0 and b) 0.15 T dc applied magnetic field for complex **2**. Temperature dependence of the c) out-of-phase phase ac susceptibility at 0.15 T dc applied magnetic field for complex **2**. Frequency dependence of the out-of-phase ac susceptibility at d) 0.15 T dc applied magnetic field for complex **1**.

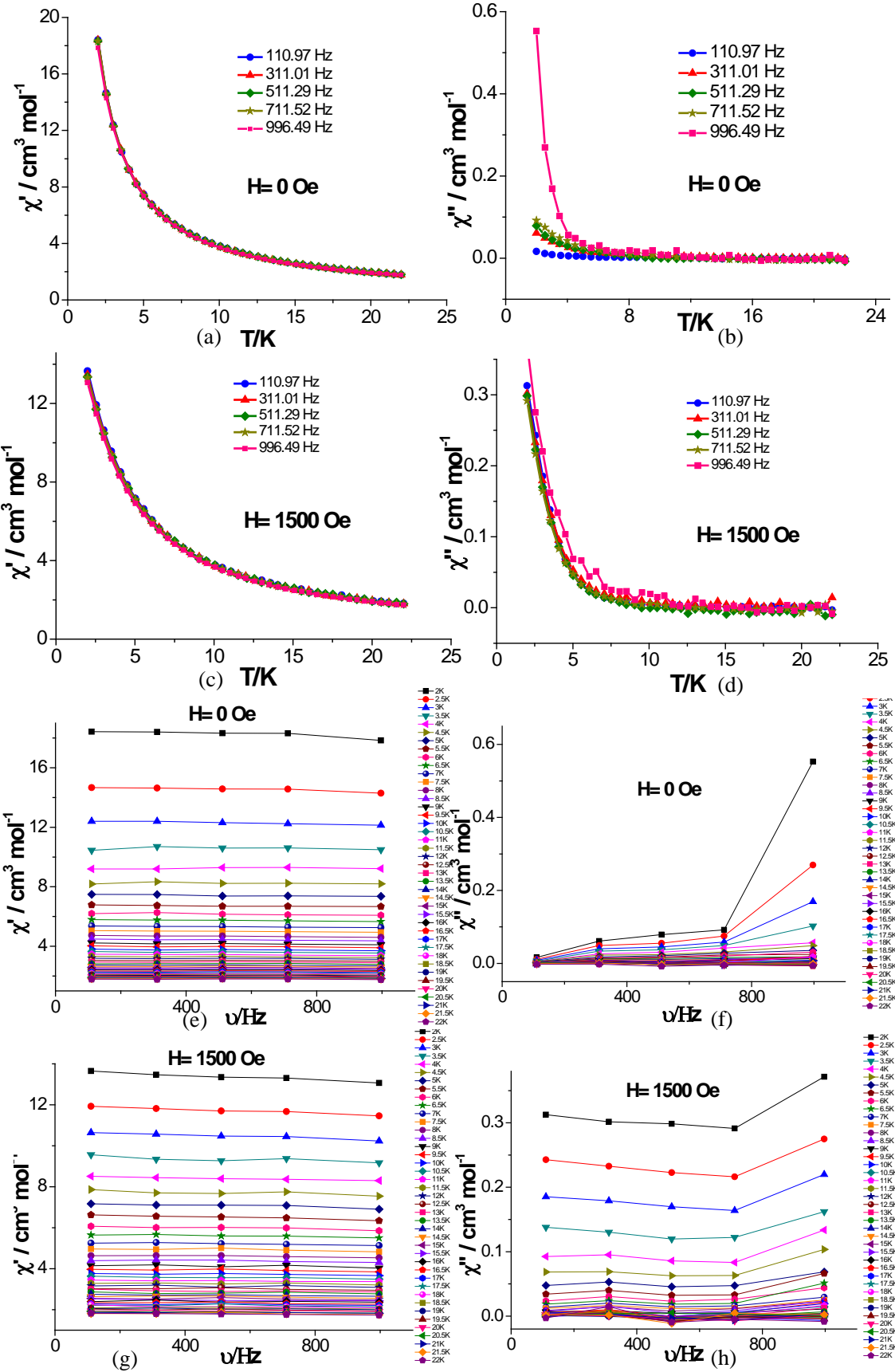


Figure S14. T-dependence in-phase {(a),(c)} and out-of-phase {(b), (d)} ac susceptibility at 0 and 0.15T respectively for **2**. Frequency-dependence in-phase {(e),(g)} and out-of-phase {(f), (h)} ac susceptibility at 0 and 0.15T respectively for **2**.

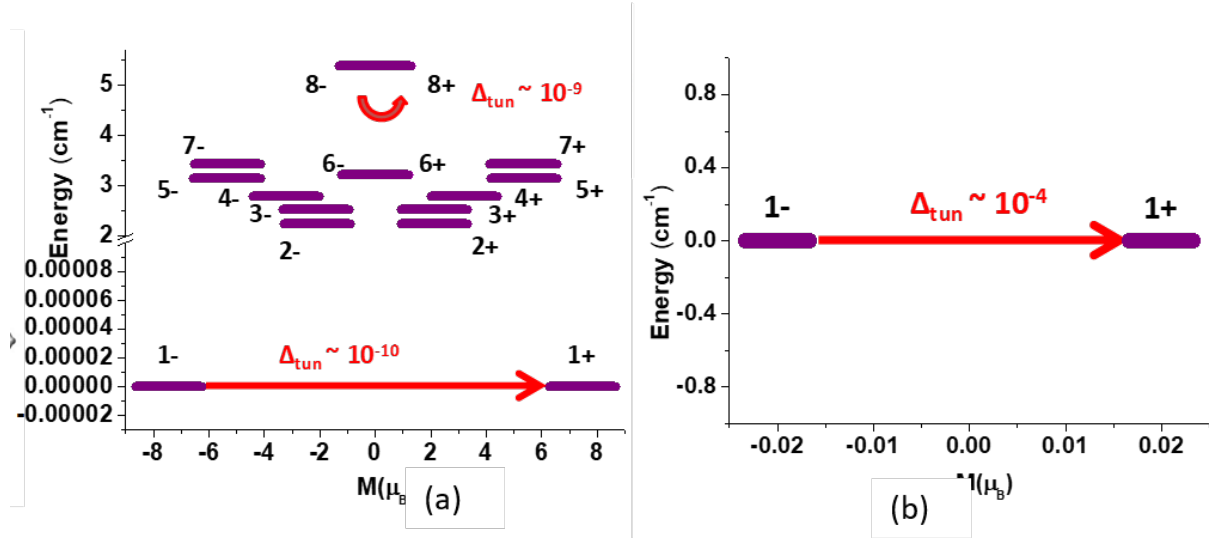


Figure S15. Low-lying exchange spectrum and the position of the magnetization blocking barrier in **1**. Tunnel splitting (denoted by red arrows) within all the low-lying eight exchange doublets is found to be negligible ($\sim 10^{-10} \text{ cm}^{-1}$, not shown for all). Every exchange state (represented by thick purple lines) has been arranged based on the corresponding magnetic moment.

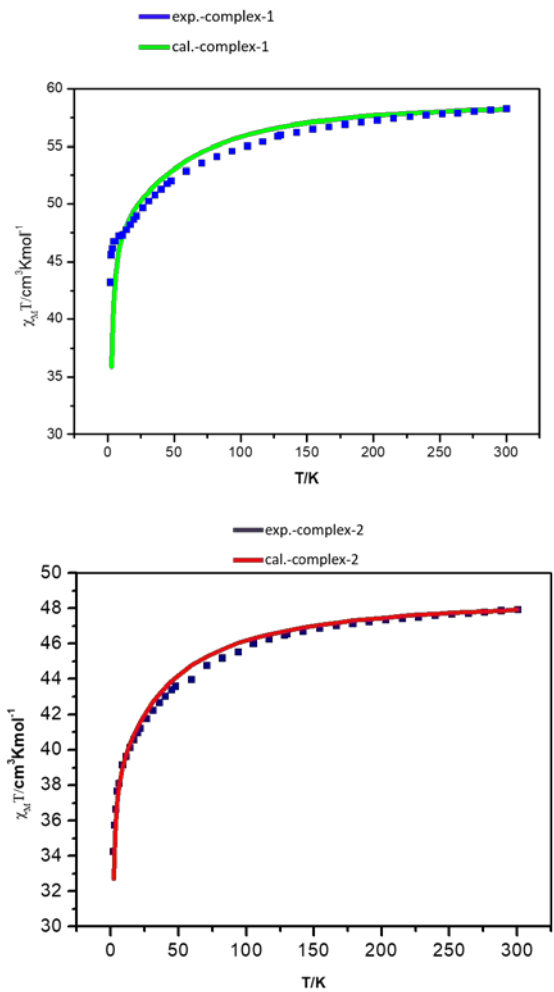


Figure S16. The Temperature T vs χT for complexes **1** and **2** fitted with POLY-ANISO module, given as separate figures with the parameters reported in table 3.